Sensors and Materials, Vol. 32, No. 4 (2020) 1427–1433
MYU Tokyo

S & M 2190

Persistent Luminescence Properties of Ti^{4+}-doped $K_2ZrSi_3O_9$ Wadeite

Yuta Iida,[1] Kenji Sawamura,[1] Kenichiro Iwasaki,[1] Takayuki Nakanishi,[2*]
Fumitaka Iwakura,[3] Yasushi Nakajima,[3] and Atsuo Yasumori[1**]

[1]Department of Materials Science and Technology, Faculty of Industrial Science and Technology,
Tokyo University of Science, 6-3-1 Niijuku, Katsushika-ku, Tokyo 125-8585, Japan
[2]National Institute for Materials Science, 1-1 Namiki, Tsukuba, Ibaraki 305-0044, Japan
[3]Daiichi Kigenso Kagaku Kogyo Co., Ltd.,
1-6-38 Hirabayashi minami, Suminoe-ku, Osaka 559-0025, Japan

(Received December 19, 2019; accepted February 28, 2020)

Keywords: persistent luminescence, zirconium, thermoluminescence

Luminescent $K_2ZrSi_3O_9$ (mineral wadeite): Ti with afterglow properties is reported for the first time. The structure analysis revealed that titanium ions were mainly substituted at the Zr^{4+} sites of $K_2ZrSi_3O_9$ as the tetravalent state. The persistent luminescence peaks at 480 nm were strongly related to two factors, namely, charge transfer (CT) transition in a Ti–O polyhedron and oxygen vacancy around Zr^{4+} sites. The $K_2ZrSi_3O_9$ wadeite including titanium ions is promising for application as a sensor using light energy storage materials.

1. Introduction

Phosphors with persistent luminescence have markedly progressed over the past decades. Thus far, these persistent luminescence materials have already been used for safety guidance signs, watch dials, and luminous paints.(1) More recently, their applications have been extended to bioimaging using temperature sensitivity,(2–4) stress imaging,(5) and security paints.(6) Since many studies suggested that persistent luminescence has been derived from the thermal release of carriers (electrons/holes) captured at trapping centers,(7) the design of host materials with trapping centers is essential for all persistent luminescence properties. As one of the great candidates for persistent luminescence phosphors, zirconia oxide derivatives have attracted attention for a long time. It is well known that pure monoclinic ZrO_2 shows 490 nm photoluminescence (PL) and persistent luminescence properties formed by ultraviolet (UV) light excitation.(8) Takahashi *et al.* also reported that the zirconia derivative $BaZrSi_3O_9$ (bazirite, $P\bar{6}m2$) shows greenish-blue persistent luminescence at around 480 nm.(9) They have also demonstrated that Ti-doped bazirite shows a higher persistent luminescence intensity than a non-Ti-doped sample.(10) These reports indicated that ZrO_6 octahedra are a key factor for luminescence and persistent luminescence properties. Here, we focused on other zirconium derivative oxides with ZrO_6 octahedra, which were expected to be a new candidate for persistent luminescence materials.

*Corresponding author: e-mail: NAKANISHI.Takayuki@nims.go.jp
**Corresponding author: e-mail: yasumori@rs.noda.tus.ac.jp
https://doi.org/10.18494/SAM.2020.2745

ISSN 0914-4935 © MYU K.K.
https://myukk.org/

In this study, the light storage ability using ZrO_6 octahedral sites of Ti-doped $K_2ZrSi_3O_9$ (wadeite) was demonstrated for the first time. The specific crystal structure of wadeite (Fig. 1) consists of three-membered Si_3O_9 rings of SiO_4 tetrahedra and coordinated ZrO_6 octahedra, via corner sharing, with K^+ occupying the cavities [the crystal graphic is drawn by VESTA[11]]. Wadeite is also expected to be a novel host crystal of persistent luminescence materials when doped with Ti. Herein, we report the PL properties of wadeite phases with various Ti concentrations. As a result, wadeite showed greenish-blue PL and persistent luminescence properties after doping Ti into Zr^{4+} sites. The fluorescence and persistent luminescence properties were evaluated. The role of Ti in the persistent luminescence properties was also determined by a thermoluminescence (TL) method. The results of this study are expected to have a significant contribution to the fields of inorganic chemistry and material design.

2. Materials and Methods

2.1 Sample preparation

The wadeite $K_2Zr_{1-x}Ti_xSi_3O_9$ was synthesized by a conventional solid-state reaction method. The starting materials, namely, ZrO_2 (99.8%, Daiichi Kigenso Kagaku Kogyo Co., Ltd.), SiO_2 (99.9%, Wako), K_2CO_3 (99.5%, Wako), and TiO_2 (98.5%, Wako) were thoroughly mixed and ground using an alumina mortar. The mixtures were placed in an alumina crucible and calcined at 800 °C for 8 h in an electric furnace under air ambient. After calcining, the mixtures were reground and pressed at 40 MPa into pellets of 10 mm φ. These pellets were placed on platinum foils and sintered at 1200 °C for 12 h in air ambient, and finally, the sintered polycrystalline samples were obtained.

2.2 Characterization

The identification results and lattice constants of the synthesized samples were examined using an X-ray diffraction (XRD) measurement system (Rigaku, Ultima III) with Cu-Kα radiation. Rietveld refinements of the samples were carried out using PDXL software (Rigaku Co.). The visual confirmation of the PL and afterglow of polycrystalline samples was carried

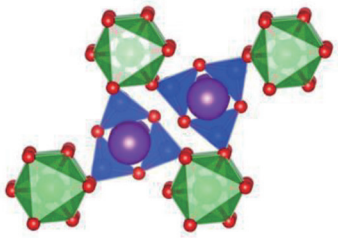

Fig. 1. (Color online) Crystal structure of wadeite: sphere, blue tetrahedron, and green octahedron correspond to K^+, SiO_4, and ZrO_6 units, respectively.

out using UV lamps with wavelengths of 254 and 300 nm, respectively. The PL and PL excitation (PLE) spectra were studied using a spectrofluorometer (JASCO, FP-6500) with a xenon lamp as an excitation source. The internal quantum yields (QYs) for saturated PL were measured using an integrated sphere measurement system. The diffuse reflection spectra were measured in the range of 200–600 nm using a UV–visible spectrometer (JASCO, V-670) with an attached integrating sphere. To evaluate the trapping center of afterglow, we measured the TL glow curves after removing the samples from the excitation source. The TL glow curves were studied using a spectrofluorometer with a xenon lamp in the temperature range of 77–300 K.

3. Results and Discussion

3.1 Sample preparation

Figure 2(a) shows the powder XRD patterns of the crystalline sample ($x = 0$) and the pattern from the Joint Committee on Powder Diffraction Standards (JCPDS). The powder XRD peak was assigned to be the wadeite-type phase by comparison with the crystallographic data of $K_2ZrSi_3O_9$ (JCPDS:43-0231). The refinement of the crystal structure revealed that the wadeite phase belonged to the hexagonal system and the space group was $P63/m$. The lattice constants were evaluated to be $a = 0.693$ and $b = 1.018$ nm. These values corresponded to those reported in the JCPDS 43-0231 ($K_2ZrSi_3O_9$). Then, the lattice constants of wadeite phases associated with the Ti^{4+} concentration were calculated by Reitveld refinement. The reliability factor of calculation was $R_{wp} = 5.9$–7.8%. The dependence of lattice constants on Ti^{4+} concentration is shown in Fig. 2(b). This result shows that the lattice constants a and c decreased with Ti^{4+} concentration. It was implied that Ti^{4+} ions were substituted at Zr^{4+} sites because the ionic radius of Ti^{4+} was smaller than that of Zr^{4+}. Thus, the target samples were successfully synthesized.

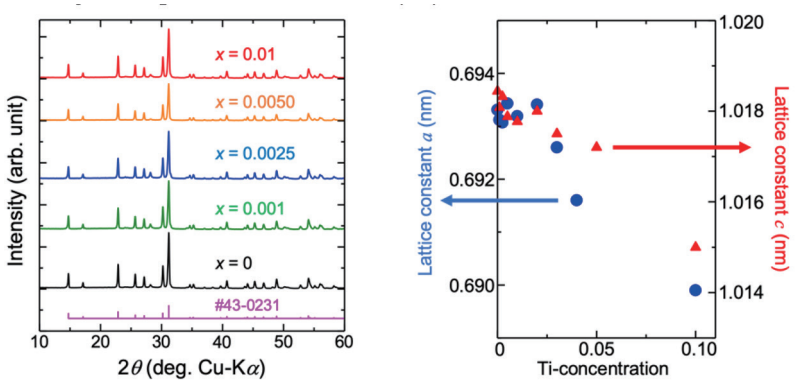

(a) (b)

Fig. 2. (Color online) (a) Powder XRD patterns of crystalline sample synthesized by sintering the stoichiometric composition of $K_2Zr_{1-x}Ti_xSi_3O_9$. (b) Relationship between lattice constants and Ti concentration in the wadeite phases.

3.2 Photoluminescence properties of Ti-doped $K_2ZrSi_3O_9$

Table 1 shows the PL of wadeite samples ($K_2Zr_{1-x}Ti_xSi_3O_9$). We could confirm very weak PL in the non-Ti-doped wadeite sample. By doping Ti at Zr sites, the PL properties were improved, and we could observe greenish-blue PL clearly.

The PL and PLE spectra of $K_2Zr_{1-x}Ti_xSi_3O_9$ are shown in Fig. 3. The broad-band photoemission in the visible greenish-blue region with a peak around 480 nm was detected in the range of x = 0–0.01. The PL intensity increased with the Ti^{4+} concentration and showed the best performance when x = 0.0025. The excitation band of the non-Ti-doped sample was only observed around 235 nm. By doping Ti, a new excitation band appeared around 300 nm. The excitation band centered at 235 nm was observed in the non-Ti-doped sample and its intensity was improved by doping Ti. Considering some literature about the PLE of zirconia derivatives,[9,10,12] this shorter excitation band was attributed to the charge transfer (CT) transition from the 2p orbits of the surrounding oxygen to the empty outer 3d orbit of Zr^{4+}/Ti^{4+} in the zirconium/titanium–oxygen octahedral unit (ZrO_6, TiO_6 unit), i.e., $O^{2-} - Zr^{4+} \rightarrow O^{-} - Zr^{3+}$ and $O^{2-} - Ti^{4+} \rightarrow O^{-} - Ti^{3+}$. On the other hand, the excitation band centered at 300 nm was only observed in Ti-doped samples. In $BaTiSi_2O_7$, Takahashi *et al.* reported that the orange PL derived from the oxygen vacancy in Ti–O polyhedral units was observed by 350 nm excitation.[12] In our case, it was considered that the broad excitation band around 300 nm was attributed to the oxygen vacancy in the TiO_6 unit.

Table 1
Photoimages of $K_2Zr_{1-x}Ti_xSi_3O_9$ under 254 nm UV irradiation.

x = 0	x = 0.001	x = 0.0025	x = 0.0050	x = 0.01
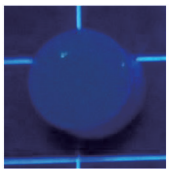	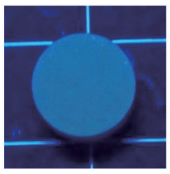		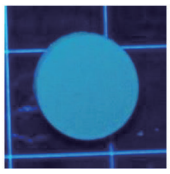	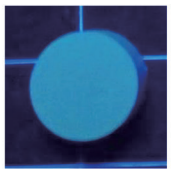

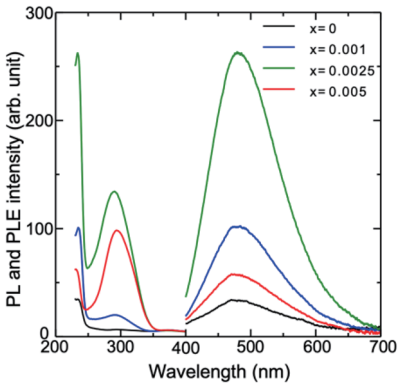

Fig. 3. (Color online) PL and PLE spectra of $K_2Zr_{1-x}Ti_xSi_3O_9$.

Figure 4 shows the relationship between Ti concentration and internal QY in $K_2Zr_{1-x}Ti_xSi_3O_9$ series. The values were improved by doping Ti and showed the best value when $x = 0.0025$. Further increasing the amount of Ti reduced the internal QY. This trend has also been confirmed in Ti-doped $BaZrSi_3O_9$ and alkaline-earth stannate crystals,[10] so it was probably due to concentration quenching.

The diffusion reflectance spectra are shown in Fig. 5. The diffusion reflectance around 300 nm decreased with Ti doping. Considering some literature about the absorption of zirconia derivatives,[9,10,12] the absorption band is ascribed to the CT transition from the 2p orbits of the surrounding oxygen ions (O^{2-}) to the empty outer 3d orbit of titanium ions (Ti^{4+}) in the titanium–oxygen octahedral (TiO_6 octahedral) unit.

3.3 Afterglow properties of Ti-doped $K_2ZrSi_3O_9$

Although the non-Ti-doped sample hardly indicated afterglow properties, the Ti-doped sample clearly showed greenish-blue afterglow in the range of $x = 0.001$–0.01. Figure 6(a)

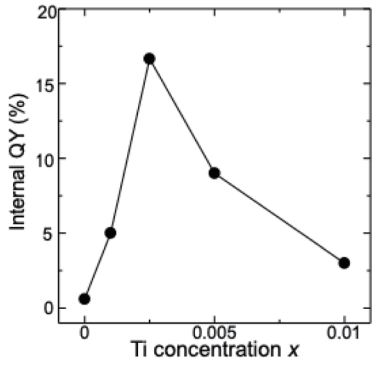

Fig. 4. (Color online) Dependence of the internal QY on Ti concentration in $K_2Zr_{1-x}Ti_xSi_3O_9$ excited at 240 nm and monitored at 400–700 nm.

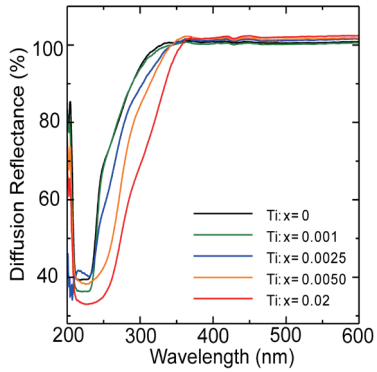

Fig. 5. (Color online) Diffusion reflectance spectra of $K_2Zr_{1-x}Ti_xSi_3O_9$.

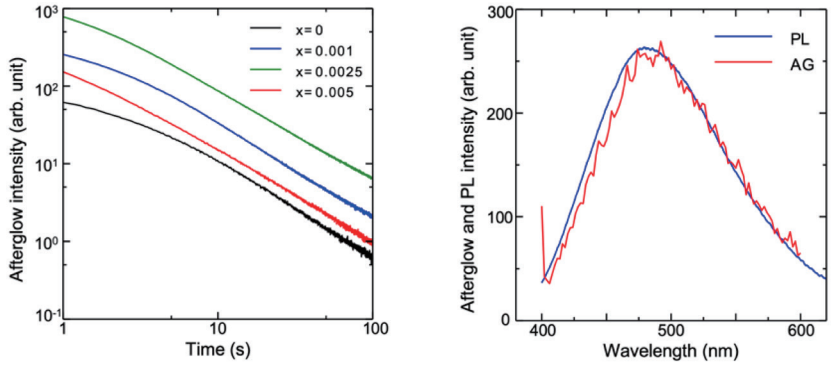

(a) (b)

Fig. 6. (Color online) (a) Afterglow decay curves (monitored at 480 nm) of $K_2Zr_{1-x}Ti_xSi_3O_9$. The samples were excited at 240 nm for 10 min before recording. (b) Afterglow PL (~2 s later) and PL profiles of $K_2Zr_{1-x}Ti_xSi_3O_9$ excited at 240 nm ($x = 0.0025$).

shows the afterglow decay curves of $K_2Zr_{1-x}Ti_xSi_3O_9$. The afterglow properties depended on Ti concentration, and the best performance was observed when $x = 0.0025$. Although we could confirm the improvement of afterglow intensity by doping Ti, there was no significant change in the shape of the afterglow decay curve. The gradient of the afterglow decay curve indicates the lifetime of afterglow. The lifetime of afterglow depended on the depth of trapping centers. The fact that the gradient of the afterglow decay curve did not change significantly implied that the doped Ti ions did not affect the trapping centers. The afterglow PL spectra of $K_2Zr_{1-x}Ti_xSi_3O_9$ ($x = 0.0025$) are shown in Fig. 6(b) with PL spectra obtained under excitation. The emission peak of afterglow was centered around 480 nm, similarly to the PL peak. This result indicates that the luminescence center of afterglow is the same as that of PL.

3.4 Evaluating the trapping centers of $K_2ZrSi_3O_9$

Since afterglow has been derived from the thermal release of carriers captured at the trapping centers, evaluating the trapping centers is important. We measured the TL spectra, which is a well-known method of evaluating the trapping centers.[13,14] Figure 7 shows the TL spectra of $K_2Zr_{1-x}Ti_xSi_3O_9$. We observed some TL peaks in each sample in the range of 78–300 K, indicating that some kind of trapping center was formed in $K_2ZrSi_3O_9$. It was crucial that some TL peaks were observed in the non-Ti-doped sample. The wadeite has two oxygen sites and could pose two types of oxygen vacancy, which form different depths of trapping center. Also, interstitial oxygen ions and metal iron could form the trapping center. Taking into account these issues, we may expect that trapping centers will mainly originate from oxygen vacancies. By doping Ti, we could confirm that each TL intensity increased. In particular, the TL peak around 100 K markedly increased and the trapping center was activated by doping Ti. On the other hand, new TL peaks and a marked peak shift were not observed by doping Ti. These results imply that the doped Ti did not form trapping centers and the depth of trapping centers was not changed by doping Ti. In this case, the oxygen vacancy around the Ti–O unit would act as not only the afterglow luminescence center but also the trapping center. In view of material chemistry, further study on novel $K_2ZrSi_3O_9$ is expected to contribute to the development of future light storage materials as advanced materials.

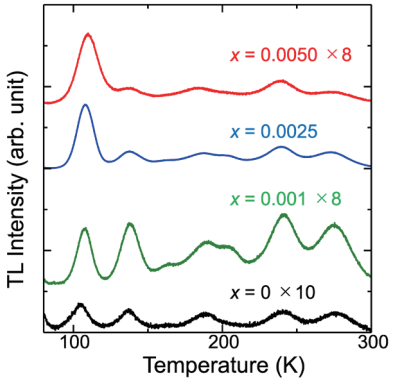

Fig. 7. (Color online) TL spectra (monitored at 480 nm) of $K_2Zr_{1-x}Ti_xSi_3O_9$ recorded at a rate of 5 K/min, after exciting the samples at 240 nm for 30 min (at 78 K).

4. Conclusion

We successfully synthesized $K_2Zr_{1-x}Ti_xSi_3O_9$ as the afterglow material for the first time by a conventional solid-state reaction method and investigated its afterglow properties. By doping Ti at Zr sites, clear greenish-blue PL and afterglow centered at 480 nm were observed at room temperature. These properties depended on Ti concentration and the best performance was observed when $x = 0.0025$. Both PL and afterglow originated from the CT transition TiO_6 unit and the oxygen vacancy related the TiO_6 unit. By evaluating TL spectra, the doped Ti did not act as the trapping center and the trapping center was attributed to the lattice defects in the host crystal such as oxygen vacancy. The information obtained by this study would contribute to the development of Zr including afterglow materials.

References

1 W. M. Yen, S. Shionoya, and H. Yamamoto: Phosphor Handbook (CRC Press, Boca Raton, 2006).
2 T. Maldiney, A. Lecointre, B. Viana, A. Bessière, M. Bessodes, D. Gourier, C. Richard, and D. Scherman: J. Am. Chem. Soc. **133** (2011) 11810. https://doi.org/10.1021/ja204504w
3 M. Pellerin, E. Glais, T. Lecuyer, J. Xu, J. Seguin, S. Tanabe, C. Chanéac, B. Viana, and C. Richard: J. Lumin. **202** (2018) 83. https://doi.org/10.1016/j.jlumin.2018.05.024
4 S. Xu, R. Chen, and C. Zheng: Adv. Mater. **28** (2016) 9920. https://doi.org/10.1002/adma.201602604
5 C. N. Xu, T. Watanabe, M. Akiyama, and X. G. Zheng: Appl. Phys. Lett. **74** (1999) 2414. https://doi.org/10.1063/1.123865
6 Y. Li, M. Gecevicius, and J. Qiu: Chem. Soc. Rev. **45** (2016) 2090. https://doi.org/10.1039/c5cs00582e
7 F. Clabau, X. Rocquefelte, S. Jobic, P. Deniard, M. Whangbo, A. Garcia, and J. Rouxel Chem. Mater. **17** (2005) 3904. https://doi.org/10.1021/cm050763r
8 Y. Cong, B. Li, S. Yue, D. Fan, and X. Wang: J. Phys. Chem. C. **113** (2009) 13974. https://doi.org/10.1021/jp8103497
9 Y. Takahashi, H. Masai, T. Fujiwara, K. Kitamura, and S. Inoue: J. Ceram. Soc. Japan **116** (2008) 357. https://doi.org/10.2109/jcersj2.116.357
10 K. Iwasaki, Y. Takahashi, H. Masai, and T. Fujiwara: Opt. Express **17** (2009) 18054. https://doi.org/10.1364/OE.17.018054
11 K. Momma, and F. Izumi: J. Appl. Cryst. **44** (2011) 1272. https://doi.org/10.1107/S0021889811038970
12 Y. Takahashi, T. Konishi, K. Soga, and T. Fujiwara: J. Ceram. Soc. Japan **116** (2008) 1104–1107. https://doi.org/10.2109/jcersj2.116.1104
13 T. Sakai, M. Koshimizu, Y. Fujimoto, D. Nakauchi, T. Yanagida, and K. Asai: Sens. Mater. **30** (2018) 1564. https://doi.org/10.18494/SAM.2018.1920
14 G. Okada, T. Kato, D. Nakauchi, K. Fukuda, and T. Yanagida: Sens. Mater. **28** (2016) 897. https://doi.org/10.18494/SAM.2016.1250